FRONT MATTER

Point-of-care applicable metabotyping using biofluid-specific electrospun MetaSAMP®s directly amenable to ambient ionization mass spectrometry

Direct metabotyping using biofluid-specific MetaSAMP®s

Authors

Margot De Spiegeleer[1], Vera Plekhova[1], Jozefien Geltmeyer[2], Ella Schoolaert[2], Beata Pomian[1], Varoon Singh[1], Kathleen Wijnant[1], Kimberly De Windt[1], Volter Paukku[1], Alexander De Loof[3], Inge Gies[4], Nathalie Michels[5], Stefaan De Henauw[3], Marilyn De Graeve[1], Karen De Clerck[2], Lynn Vanhaecke[1,6,†,*]

Affiliations

[1]Laboratory of Integrative Metabolomics, Department of Translational Physiology, Infectiology and Public Health, Ghent University, Belgium.

[2]Department of Materials, Textiles and Chemical Engineering, Faculty of Engineering and Architecture, Ghent University, Belgium.

[3]Department of Public Health and Primary Care, Faculty of Medicine and Health Sciences, Ghent University, Belgium.

[4]Department of Pediatrics, Vrije Universiteit Brussel (VUB), Universitair Ziekenhuis Brussel (UZ Brussel), Belgium.

[5]Department of Developmental, Personality and Social Psychology, Ghent University, Belgium.

[6]Institute for Global Food Security, School of Biological Sciences, Queen's University, United Kingdom.

***Corresponding author**

Prof. Dr. Lynn Vanhaecke

ORCID 0000-0003-0400-2188

Laboratory of Integrative Metabolomics

Department of Translational Physiology, Infectiology, and Public Health

Faculty of Veterinary Medicine, Ghent University,

Salisburylaan 133, B-9820 Merelbeke, Belgium

Tel: +32 9 264 74 57

E-mail: Lynn.Vanhaecke@UGent.be

Abstract

While rapid analysis of the human biofluid metabolome is now possible using ambient ionization mass spectrometry (AIMS), these procedures are hampered by in-source matrix effects and reduced sample stability impeding metabolome coverage while remaining relatively labor-intensive. In this study, we aimed at developing biofluid-specific metabolome sampling membranes (MetaSAMP®s, WO2021/191467) that offer a directly applicable and stabilizing substrate for AIMS. Customized rectal, salivary and urinary MetaSAMP®s consisting of multilayered electrospun nanofibrous membranes of blended hydrophilic (polyvinylpyrrolidone and polyacrylonitrile) and lipophilic (polystyrene) polymers supported adequate metabolite ab- , ad-, and desorption. Moreover, MetaSAMP® demonstrated superior metabolome coverage and transport stability compared to crude biofluid analysis and was successfully validated in two pediatric cohorts (MetaBEAse, *n*=234, feces and urine; OPERA, *n*=138, saliva). By integrating anthropometric and (patho)physiological with MetaSAMP®-AIMS metabolome data, we obtained significant weight-driven predictions and clinical correlations. In conclusion, MetaSAMP® holds great clinical application potential for on-the-spot metabolic health stratification.

Teaser

Customized biofluid-specific MetaSAMP®s enable superior metabolome coverage and stability for direct health stratification.

MAIN TEXT

Introduction

To date, metabolomics of human biofluids is emerging as a promising biofocus as it provides advantages that classical diagnostics do not, following discovery of a suite of clinically relevant biomarkers that are simultaneously affected by disease while contributing to the elucidation of metabolic pathways underlying particular phenotypes of health and disease (i.e., metabotyping) (*1–3*). The most urgent application of metabolomics remains the identification of pathologies in children as early-infancy exposures, including nutrition and illness severely impact adult health and functionality as well (*4*). In this respect, metabolite patterns offer a valid tool to profile individuals (*5*) at risk of developing e.g., the metabolic sequelae coinciding the global rise in overweight and obesity (*6*) by discerning between metabolically healthy and unhealthy phenotypes and predict future risks of developing co-morbidities such as (pre)diabetes, metabolic syndrome, etc. (*2, 7–10*).

The urinary and fecal metabolomes have been popularized as they reflect both exogenous and endogenous metabolic products (*11*), as well as complex interactions between dietary intake, gut microbiome and host (*12*). Salivary metabolites on the other hand, largely mirror those in blood and may thus reflect many pathophysiological and nutritional changes, as well as exposure to medication and environmental factors (*13*). Major bottlenecks in large metabolomics cohort studies remain the collection, transport, storage and sample preparation of biofluids. Indeed, ongoing (bio)chemical reactions following sample collection, long-term preservation and extraction may substantially introduce metabolome alteration (*12*, *14*) and misleading interpretations, while the addition of chemical preservatives during shipping, storage and extraction causes metabolome contamination by adduct formation and/or ion pairing (*15*).

The typical workflow used in conventional biofluid metabolomics comprises multiple time-consuming steps including sample collection and pretreatment such as lyophilization, extraction and chromatographic separation, etc., resulting in low sample throughput (ca. 60/day) and high costs (> 200 euro/analysis) (*16*). During the last decades, instrumental advances have allowed the integration of near-real-time surface sampling or ambient ionization (AI) of matrices in their native analyte environment (*17–19*). Laser ablation coupled to rapid evaporative ionization mass spectrometry (REIMS), termed laser-assisted REIMS (LA-REIMS), is among the few ambient ionization-based techniques that have found their way into the clinic both *in vivo* and *ex vivo* (*16*, *20*). LA-REIMS uses a sample-focused laser beam that excites the most intense vibrational band (oxygen-hydrogen stretching mode) of water molecules present in the sample, initiating ablation heat and causing evaporation. The resulting analyte-containing aerosol is aspirated towards the MS under the instrument's vacuum where it is mixed with a solvent and collides with a heated collision surface to form gas-phase ions for analysis (*16*, *20*). To date, LA-REIMS is the only AIMS platform that has been successfully employed for the automated analysis of a range of crude biofluids, including feces, saliva, urine, etc. (*1*). Indeed, LA-REIMS enables an analysis rate of only few min/sample, and demonstrates significant congruencies with mass spectra obtained by conventional metabolomics (*16*, *21*, *22*). Current challenges in direct LA-REIMS-based crude biofluid analysis are the existence of matrix effects and reduced ionization efficiency, resulting in a decreased selectivity and thus metabolome coverage (*23*). Moreover, biofluid collection may hamper a direct sampling-to-MS result workflow (*1*), because the need to wait for e.g., defecation prevents immediate sample availability. A sampling device that allows the integration of sampling, sample preparation and presenting the sample for direct metabolomics analysis, would offer a substantial advance compared to crude biofluid analysis, because it would largely circumvent these challenges.

In this study, we aimed at developing, optimizing and benchmarking novel biofluid-specific samplers (MetaSAMP®s, WO2021/191467) for direct rapid AIMS-based metabotyping (Fig. 1A). Our MetaSAMP®s consist of nanofibrous membranes customized both in terms of polymer composition, ratio and fiber diameter by electrospinning (ES) towards optimal biofluid-specific (feces, saliva and urine) metabolome sampling, extraction, and stabilization. ES is a simple and versatile technology that uses electrostatic forces to produce (nano)fibrous membranes with controllable compositions (*24*, *25*). The typical porous bed structure of electrospun membranes enables analyte enrichment due to highly efficient mass transfer between biofluids and the polymerous (nano)fibers, which act as sorbents, facilitating metabolite microextraction (*26*, *27*). The possibility of including specific chemical moieties offers a means to enhance the extraction coverage of analytes bearing a broad range of polarities (*28*). Moreover, biocompatible polymers such as polyacrylonitrile (PAN) are also suitable for ES, which allows for *in vivo* usage while supporting the exclusion of macromolecules (*29*). The MetaSAMP®s may be configured as a medical swab or a kit with an integrated electrospun membrane that is directly amenable to our established rapid LA-REIMS platform (*1*). We also confirmed the ability of MetaSAMP®s to stabilize the biofluid-specific metabolome, increasing transport ease and duration. Finally, the clinical applicability and superior performance of our MetaSAMP®s relative to the analysis of crude biofluids, were assessed *ex vivo* in 2 pediatric cohorts (MetaBEAse and OPERA). As such, we have demonstrated that direct MetaSAMP®-based biofluid metabotyping may have far-reaching potential as a future medical device.

Results

Optimized electrospun membranes for biofluid-specific metabolic fingerprinting: MetaSAMP®s

The development of our biofluid-specific metabolome sampling MetaSAMP®s started by tuning the configuration and chemical composition of each extractive core membrane (feces, saliva and urine, Fig. 1B) towards maximal metabolome coverage following LA-REIMS analysis (wide logP span and molecular feature count) and repeatability (as % of molecular features with a CV≤30%). Hereto, the electrospun core membranes were fabricated using a rotating drum collector (Fig. 1C) on an aluminium support layer (Fig. 1B). Because the superiority of materials with a hydrophilic-lipophilic balance (HLB) as comprehensive metabolome extraction sorbents has been reported (*28*, *30*), we selected two relevant HLB polymers (PVP and PS) for our core membranes. As feces (and rectal content) are more heterogenous, complex and richer biofluids than saliva (*13*) or urine (*11*), the rectal MetaSAMP® optimization was prioritized. Following impregnation with

porcine rectal content, different compositions were evaluated for their metabolome coverage using LA-REIMS analysis (Supplementary Note 1). The usage of porcine rectal content was rationalized based on similarities in nutrition and metabolism between pigs and humans (*31*). Additionally, the LA-REIMS settings were further optimized for the rectal MetaSAMP® using a design of experiments (Supplementary Note 1). Significance (ANOVA FDR-adjusted p=0.012 and p<0.001, F=14.62 and 25.35, df=5) was detected for higher scan time and solvent flow rate. The optimal values were obtained by maximizing metabolome coverage, molecular feature signal intensity and repeatability, resulting in a scan time of 0.7 scans s^{-1} and a solvent flow rate of 250 µL min^{-1} (Supplementary Table 1). It was observed that a balanced blend of PVP/PS (50/50, *w/w*) significantly outperformed (ANOVA FDR-adjusted p=9.03e^{-8}, F=41.44, df=19) the other compositions tested in terms of metabolome coverage (Supplementary Note 1, Supplementary Figs. 1-2). Consequently, the HLB of the core membrane's compositional fibers was demonstrated through modulated differential scanning calorimetry. Separate glass transition temperatures (Tg) could be assigned to carbonyl- (PVP) and benzene-rich (PS) moieties (*32*) (Supplementary Fig. 3).

Hereafter, electrospun core extractive membranes were optimized in a similar fashion for saliva and urine. Initial experiments demonstrated that a higher relative weight% of PS *vs.* PVP, and a higher total polymer weight%, increased the metabolome coverage upon LA-REIMS analysis. Instrumental settings for LA-REIMS analysis of impregnated electrospun membranes with saliva and urine were the same as our previously biofluid-specific optimized protocol (*1*) (Supplementary Table 1). The markedly higher percentage of PS in the PVP/PS core membrane layers for sampling urine and saliva compared to rectal sampling however resulted in longer biofluid residence times, as demonstrated by contact angle measurements (CAM) (130±10°). The latter could be ascribed to the more aqueous nature of urine and saliva. Because an increased biofluid residence time was observed to bring about more variable impregnation times, we additionally evaluated the inclusion of the highly polar PAN polymer in the core extractive membranes for urine and saliva by comparing blends of PVP/PS (0-20% PVP) with PVP/PS/PAN blends (5-20% PVP and 5-10% PAN), as this polymer may increase the wettability (*33*) and thus speed of analysis upon inclusion. Both those core membrane compositions were evaluated first through scanning electron microscopy (SEM) for their network stability upon impregnation with saliva and urine. The SEM images revealed no visible damage to the electrospun fibrous core blends, suggesting morphological integrity even after prolonged biofluid exposure (> 15 min) (Supplementary Fig. 4), hinting towards efficient analyte interaction. Additionally, fiber size distributions were compared for the various compositions. It was observed that a higher amount of PVP in both blends, i.e., 10-20% PVP for

the PVP/PS membranes and 20% PVP and 10% PAN, resulted in a more homogenous size distribution, benefitting the reproducibility of LA-REIMS metabolomics analysis.

Next, we investigated the potential of a PAN cover layer on top of our core extractive membrane considering the future rectal MetaSAMP®'s *in vivo* usage as a medical swab. Indeed, aside from its high polarity and thus wetting capabilities for aqueous matrices (*33*), PAN is also a biocompatible polymer with documented *in vivo* applications (*34*, *35*) that has previously been demonstrated to facilitate selective transport of small molecules to extractive polymers by partially diminishing surface (bio)fouling mechanisms for molecules >1.5 kDa and completely preventing access to molecules >7 kDa (*29*, *36*). As a result, a PAN cover layer was hypothesized to enhance extractive core membrane stability as surface functionalities of the PVP/PS microporous core are expected to be less susceptible to oxygen or moisture in its presence. For this experiment, pooled QC fecal samples were used, enabling the evaluation of our future target matrix and thus reproducibility of the entire analysis protocol best. Indeed, feces shows substantial similarity with rectal content with respect to bacterial community structure and functionality (*37*, *38*). Hereto, PAN was tested at various concentrations (5-15%, *w/w*) and evaluated for its solution viscosity, quality of the PAN electrospun fiber network and fiber size distribution (Supplementary Fig. 5 and Supplementary Table 2). Optimal small molecule sampling and subsequent analysis were strived at by retaining the average fiber diameter and its distribution as low as possible in effectively excluding macromolecules like proteins and DNA. The combination of an acceptable average fiber diameter of 384 nm (Supplementary Fig. 6) and a smooth fiber network without bead formation as observed by SEM (Supplementary Fig. 7), which might hamper metabolome sampling and analysis, rationalized our choice to use 10% (*w/w*) PAN in further experiments. To confirm the optimal position of the electrospun PAN layer, the effect of varying its position relative to the extractive core PVP/PS membrane was tested. The effects of an electrospun PAN cover layer added to the PVP/PS electrospun core membrane both with and without including PAN as a bottom layer on the Al support were examined in terms of metabolic coverage (ranging from 50-1200 Da) and repeatability. To identify which metabolite classes were impacted by the presence of PAN cover and bottom layers, the measurable mass range was subdivided into six subsets, including a subset covering 50-200 Da, encompassing low-molecular-weight metabolites such as carbohydrates and short-chain fatty acids; two subsets covering 200-600 Da, encompassing medium-, long- and very-long-chain fatty acids as well as amino acids, diacylglycerols, and sphingolipids; two subsets covering 600-1000 Da, encompassing phospholipids a.o. (*16*, *18*, *39*), and a subset covering 1000-1200 Da, mainly encompassing saccharolipids and glycosphingolipids (*40*). Indeed, from a metabolic health perspective(*2*), metabolite classes covering all those mass ranges are relevant. The

impregnated electrospun core membranes covered by an additional electrospun PAN layer gave significantly higher metabolome coverage following LA-REIMS analysis and signal intensities compared to the analysis of the crude biofluid (Supplementary Table 3 and Supplementary Fig. 8). It was also observed that the PAN cover layer enhanced the spreading and therefore penetration of fecal water (Supplementary Fig. 9) as confirmed by smaller CAMs (50±2° versus 144±4°) (Supplementary Table 4 and Supplementary Fig. 10). As a result, the increased hydrophilicity/wettability brought about by the electrospun PAN cover layer promotes beneficial chemical and physical interactions between biofluid metabolites and the core extractive membrane (*26*).

Because the metabolome core extractive capabilities were expected to be affected by the addition of the biocompatible filtering PAN cover layer, a second optimisation round was initiated for obtaining the final composition of each biofluid-specific MetaSAMP®. To this end, average fiber diameter and morphology, signal intensity, metabolome coverage and repeatability were evaluated as endpoints. The core extractive membrane composed of PVP/PS (60/40, *w/w*) with 8% (*w/w*) total polymer weight% covered by a PAN layer and impregnated with fecal water showed statistically significant higher intensity values (ANOVA FDR-adjusted p=0.017, F=13.95, df=1) as well as improved repeatability and metabolome coverage (ANOVA FDR-adjusted p=0.042, F=28.99, df=1) upon LA-REIMS analysis compared to analysis of the crude fecal water (Supplementary Table 5). The core layers comprising PVP/PS (10/90) and PVP/PS/PAN (20/70/10) both with 14% (*w/w*) total polymer weight% and covered with an electrospun PAN layer, were selected as the optimal substrates for LA-REIMS analysis of saliva and urine, respectively, in terms of higher metabolome coverage and repeatability (95% and 97% of features with CV≤30% for saliva and urine, respectively) (Supplementary Table 6) compared to crude analysis of saliva and urine. In conclusion, our three final optimized rectal, salivary and urinary MetaSAMP®s comprised of, respectively, blends of electrospun PVP/PS 60/40, PVP/PS 10/90, and PVP/PS/PAN 20/70/10 covered with an electrospun PAN layer.

Direct MetaSAMP®-LA-REIMS offers a richer metabolic fingerprint than crude biofluid LA-REIMS

Following optimization, we aimed at demonstrating the advantages of direct MetaSAMP®-LA-REIMS metabolic fingerprinting compared to crude biofluid LA-REIMS analysis in terms of metabolome coverage using impregnated rectal, salivary and urinary MetaSAMPs® from participant overweight children (n=3, IOTF>0, MetaBEAse cohort for the rectal and urinary MetaSAMP® and OPERA cohort (*41*) for the salivary MetaSAMP®) (Table 1). Richer mass spectra

and higher overall signal intensities were observed in impregnated MetaSAMP®s compared to the crude biofluid LA-REIMS metabolic fingerprints (Fig. 2, A-C). Additionally, since metabolite classes covering the aforementioned mass ranges are clinically relevant with regard to the metabolic disturbances underlying overweight and obesity (*2*), metabolome coverage (pooled QC samples, *n*=3) was also evaluated throughout the different mass ranges. As such, palmitic acid (fatty acid, *m/z* value of 255.24 Da, logP 6.4), 1-heptadecanoyl-2-(9Z,12Z,15Z-octadecatrienoyl)-sn-glycerol (glycerolipid, *m/z* value of 603.48 Da, logP 13.4) (Fig. 2A) and a putatively identified lipid (ceramide sphingolipid or phosphoethanolamine glycerophospholipid, *m/z* value of 736.50 Da) (Fig. 2A), were detected by our MetaSAMP®-LA-REIMS. As demonstrated via radar charts for each of the mass ranges, higher coverage was noted upon analysis with the biofluid-specific MetaSAMP®s as compared to the crude biofluids (Fig. 2, A-C) for most mass ranges. In conclusion, our optimized biofluid-specific MetaSAMP®s confirmed superior metabolome coverage across a broad mass range (50-1200 Da) and wide logP span compared to the analysis of crude biofluids.

Biofluid-specific MetaSAMPs® improve short-term metabolome stability and speed

Biofluid collection and transport, especially in large cohorts, is not straightforward. In the case of stool samples, the need to wait for defecation prevents the direct analysis, inferring the need of biobanking (and thus freezing). The addition of chemical preservatives to crude biofluids for shipping and storage stability negatively impacts the metabolome's accuracy (*12*, *14*). Our optimized rectal, salivary and urinary MetaSAMP®s were hypothesized to conserve a more accurate snapshot of the metabolome during storage and are directly amenable to sample preparation-free metabolomics analysis, as such lowering the individual time and cost per analysis. The storage period was set at 48h, which corresponds to the maximum transport duration from the patient's home or physician's office to the laboratory in Western countries (e.g., with courier services). To address this, metabolome coverage and repeatability based on crude biofluid fingerprinting (pooled QC samples, *n*=6) and their corresponding impregnated MetaSAMP®s were measured at RT 22±2°C and 4°C and the total sampling and analysis times were recorded. Closer correlations in the LA-REIMS results were observed between 48h stored samples and those analyzed immediately after collection using the optimized MetaSAMPs® stored at 4°C when compared to the corresponding correlations of the data obtained with their crude counterparts (Fig. 3A). At RT, however, both crude biofluids and MetaSAMPs® brought about substantial metabolome changes as confirmed by low repeatability values (<50% of features with CV≤30%). Subsequently, intraclass correlation coefficients (ICC) intervals were computed to investigate metabolome variation

between time points, considering molecular features with ICC values ≤0.4 as more unstable over time(*42*). Upon storage at 4°C, 1371 (feces) versus 1850 (rectal MetaSAMP®), 2460 (saliva) versus 3397 (salivary MetaSAMP®) and 2677 (urine) versus 2721 (urinary MetaSAMP®) molecular features remained stable (ICC>0.4) (Fig. 3B). Moreover, the total analysis time of the optimized biofluid-specific MetaSAMP®-LA-REIMS methodology was recorded as <20 min per sample (<15 min for sampling incl. impregnation and 5 min for the LA-REIMS analysis workflow) aside from the transport time. In conclusion, our MetaSAMP®s generally demonstrated a superior number of stable molecular features over time and provide an efficient means for rapid LA-REIMS-based metabotyping.

Direct biofluid-specific MetaSAMP®-LA-REIMS is a clinically valid metabotyping tool

Metabolomics analysis has substantial value in a plethora of metabolic and food-related diseases (*2*, *43*). Metabolite patterns could therefore offer a valid tool to profile individuals at high risk of developing e.g., obesity-related metabolic diseases, i.e., discerning between metabolically healthy and unhealthy phenotypes already at young age (*2*, *5*). To provide proof-of-principle for the clinical potential of our MetaSAMP®-LA-REIMS in childhood overweight and obesity, MetaSAMP®-derived metabolic fingerprints of biofluids obtained in two pediatric cohorts: MetaBEAse (feces and urine of children aged 6-12 years) and OPERA (*41*) (saliva of children aged 6-16 years) (Table 1), were investigated in terms of discrimination and predictive potential. For this purpose, a large set of anthropometric and clinical measurements were performed (Table 1) to link potentially relevant metabolite discrepancies in overweight and obese children and pathophysiological processes.

First, the discriminative and predictive performance of LA-REIMS analysis was compared between crude biofluids and their impregnated MetaSAMP®s. By doing so, more subtle effects related to subclinical pathology, i.e., metabolic perturbations due to increased weight and/or adiposity, were visualized by valid orthogonal projection to latent structures discriminant analysis (OPLS-DA) models using the international obesity BMI cutoff for thinness, overweight and obesity (IOTF) as a classifier (Fig. 4, A-C). Interestingly, a similar or even greater number of molecular features that were significantly differentiated based on their value of variable influence on projection for the OPLS-DA models constructed (Supplementary Table 7) were retrieved for the analysis of the MetaSAMP®s as compared to that of the crude biofluids. The same was noted for the validation parameters (CV-ANOVA $p< 0.05$, good permutation testing (n=100), goodness-of-fit of and predictive performance of the model reflected by R^2(cum)>0.8 and Q^2(cum)>0.4 for biological data), respectively (Supplementary Table 7). These findings provide evidence that

discriminative categorization based on metabolic fingerprints was mostly superior using the biofluid-specific MetaSAMP®-LA-REIMS methodology. Furthermore, its predictive potential for overweight classification using IOTF scores was assessed by logistic regression. This approach was only applied to the MetaBEAse cohort data because the sample size of the OPERA cohort (n=101) did not sustain good model building (*44*). Metabolic fingerprints detected by rectal (Fig. 4D) and urinary (Fig. 4E) MetaSAMP®-LA-REIMS analyses enabled predictive IOTF classification. We observed strong predictive potential (area under the curve (AUC) range 0.84-0.96) when all overweight (including obese) children as well as only obese children were included and compared to a balanced number of normal weight children, suggesting the early onset, i.e., already in overweight (not yet obese) children, of metabolic divergences (*2*).

To further clinically validate our MetaSAMP®-LA-REIMS metabotyping approach, Spearman correlations were calculated between normalized levels of molecular features captured with each biofluid-specific MetaSAMP® and anthropometric and clinical measurements from both cohorts (MetaBEAse and OPERA). Interestingly, among anthropometrics, adiposity measures (BMI-*z*, IOTF, waist circumference (WC) and waist-to-height ratio (WHR)) that are related closely to overweight metabotypes (*45*) showed the highest Spearman ρ-values with fecal, salivary and urinary metabolic profiles in both cohorts (Fig. 4, F-H). A number of clinically relevant end points, i.e., lipid, glycemic, inflammatory and hormonal blood markers, showed moderate to good correlations (Spearman ρ-values 0.4-0.6) (*46*) with biofluid-specific MetaSAMP®-derived metabolic fingerprints. For instance, glucose and insulin (-like growth factor 1) in blood, which have been associated with insulin resistance (*47*), and sex-hormone binding globulin and dehydroepiandrosterone sulphate, which have been negatively associated with adiposity and low-grade inflammation in childhood obesity (*48*, *49*), correlated well with rectal and urinary MetaSAMP®-derived fingerprints (Spearman ρ-values up to 0.5, Fig. 4, F and G) (MetaBEAse cohort). Adipokine hormones with appetite suppressing and initiating effects, such as leptin and ghrelin, respectively (*50*), revealed moderate to good correlations (Spearman ρ-values up to 0.4, Fig. 4H) with metabolic fingerprints obtained by our salivary MetaSAMP® (OPERA cohort), and hence were influenced by adiposity and insulin sensitivity (*51*). Collectively, these results suggest that our MetaSAMP®s allow capturing multiple clinically relevant metabolites of energy, immune and lipid metabolism.

As a final step in demonstrating the clinical potential of our MetaSAMP®-LA-REIMS, the identification of molecular features that showed significant (p<0.05, Wilcoxon rank-sum test) Spearman correlations with anthropometric and/or clinical parameters based on MetaSAMP®-LA-REIMS analysis was pursued. We focused on the rectal MetaSAMP® data (MetaBEAse cohort)

because stool comprises the most complex matrix and is considered most relevant to capture gut-microbiome-diet interactions (*12*). This is, the role of the microbiome and its metabolites in obesity has been ubiquitously reported in literature (*2*, *52–54*). Hierarchical Ward-linkage clustering analysis was used to unveil unique molecular features clustering according to their shared correlation structure (Fig. 5A). Annotation of potentially clinically relevant molecular features originating from the rectal MetaSAMP®-LA-REIMS fingerprints was realized (see methods and Supplementary Table 8). Subsequently, we assessed if those metabolites significantly (p<0.05, Wilcoxon rank-sum test with continuity correction or Kruskal-Wallis test with Dunn's post-hoc test) changed between different weight groups (Fig. 5B). Out of the 81 molecular features determined with rectal MetaSAMP®-LA-REIMS in negative ion mode (Fig. 5A), 8 metabolites were found to correlate with and contribute to the discrimination of weight classification in children (Fig. 5B).

Physicochemically diverse clinically relevant metabolites can be reproducibly detected using rectal MetaSAMP®-LA-REIMS

Finally, in assessing the future clinical implementation of MetaSAMP®s, a targeted approach was implemented using the rectal MetaSAMP® on a selection of clinically relevant metabolites in (childhood) overweight and obesity (*2*) according to FDA recommendations(*55*). The latter was performed with analytical standards that were selected based on their plausible natural occurrence in feces (*56*) covering a broad polarity and mass range (100-1200 Da and logP of -4 to 13, Supplementary Table 9). The targeted detectability, technical precision, repeatability and intermediate precision of these analytes were determined by applying 3 consecutive ablation events per membrane piece (n=5) on different days and calculating the number of molecular features upon LA-REIMS analysis (Supplementary Tables 9 and 10). Additionally, the standards were spiked directly onto the rectal MetaSAMP® (Supplementary Table 11) and, hereafter, onto the impregnated rectal MetaSAMP®s (Supplementary Table 12) using a pooled sample (from MetaBEAse controls, n=3). Standards spiked directly onto the rectal MetaSAMP®s, displayed intra- and interassay CVs <30% for 9 and 7 out of 11 metabolites initially detected, respectively. In conclusion, In conclusion, our results showcase that a diverse range of clinically relevant metabolites may be sufficiently reproducibly detected using rectal MetaSAMP®-LA-REIMS.

Discussion

In this work, customized biofluid-specific metabolome samplers, called MetaSAMP®s, were developed for direct user-friendly sampling, extraction and stabilization of complex human biofluids including feces, saliva and urine. The hyphenation of these optimized MetaSAMP®s with our automated LA-REIMS platform (*1*) enables direct sampling and analysis of the respective metabolomes in less than 20 min per sample (Fig. 1A) and provides a richer and more stable reflection of the biofluid-specific metabolome as compared to crude biofluid analysis. Indeed, the MetaSAMP®-LA-REIMS metabotyping approach represents a superior alternative to crude biofluid LA-REIMS analysis regarding on-the-spot metabolic health stratification and holds great potential for usage in large cohort metabolomics studies. We have therefore successfully evaluated its clinical implementation in the context of childhood obesity pandemic (*6*) using fecal, salivary and urinary metabotyping in samples obtained from two pediatric cohorts (MetaBEAse and OPERA). Although our MetaSAMP®-LA-REIMS methodology centers on untargeted metabolic fingerprinting using HRMS, we also demonstrated reproducible targeted analysis of a selection of physicochemically diverse metabolic disease-related metabolites.

The respective biofluid-specific rectal, salivary and urinary MetaSAMP®s comprised of an extractive core layer that was optimized towards maximal metabolome coverage as a blend of HLB electrospun nanofibrous polymers, i.e., PVP/PS 60/40, PVP/PS 10/90, and PVP/PS/PAN 20/70/10, covered with an electrospun PAN layer (Fig. 1B). We have provided evidence that these dual HLB properties, together with the high surface area and interconnectivity of the open microporous electrospun network, make the MetaSAMP®s' core extractive membranes excellent substrates for the enrichment, desorption and ionization of analytes with a broad physicochemical diversity in terms of characteristics such as size and polarity (*m/z* range 100–1200 and logP of -4-13) (Fig. 2). Indeed, Bian and Olesik (*57*) already reported that electrospun nanofibrous membranes may serve as an excellent substrate for a selection of small drug molecule analysis because of the nature of their microporous network, while different HLB-based extractive sampling approaches have been described (*28*) which have proven beneficial for subsequent MS-based analysis of a physiochemically broad range of metabolites. In contrast to the rectal and salivary core extractive MetaSAMP® membranes, we found that for the urinary core membrane, a blend of PVP, PS and PAN was most favorable, given the very hydrophilic nature of the waste products that comprise the urinary metabolome (*58*). Indeed, PAN is a polar polymer with wetting capabilities (*33*) that has proven advantageous in diminishing fragmentation and background noise for low molecular masses (*57*). The markedly higher fraction of PS in the salivary and urinary MetaSAMP®s resulted in a more extensive metabolome coverage, especially for the higher *m/z* ranges in which more lipids reside which are relatively less concentrated and hence more difficult to selectively extract from

such polar matrices (*59*). Furthermore, introducing the biocompatible polymer PAN (*34*, *35*) as a cover layer (*29*) reduces biofouling due to restricting access to relatively large (macro)molecules such as DNA and proteins (*29*), as shown through CAMs. Moreover, it facilitates the impregnation of aqueous biofluids into the relatively hydrophobic extractive core layer. Indeed, we observed an increased metabolome recovery and precision upon introduction of an electrospun PAN cover layer. This may be ascribed to the advantageous complementary action of the large (micrometer scale), open pores (*30*) of the core network of the nanofibrous PVP/PS(/PAN) membrane that ad- and absorbs small molecules, and the nanofibrous PAN exclusion layer that prevents the interaction of macromolecules with this nanofibrous network (*29*), most likely resulting in reduced matrix interferences upon LA-REIMS analysis of the MetaSAMP®s. Finally, as also reported by Bian and Olesik, the porosity and very high specific surface area that are inherent to electrospun membranes are especially valuable when coupled to laser-based desorption and ionization (*57*). Indeed, the observation of increased *m/z* signal intensities throughout the different *m/z* mass ranges following MetaSAMP®-LA-REIMS analysis in comparison to crude biofluid LA-REIMS analysis corroborate their findings on fast and efficient energy transfer and dissipation, boosting desorption and ionization when using electrospun nanofibrous substrates (*57*).

The fully optimized biofluid-specific MetaSAMP®s increased the short-term biofluid metabolome stability (at 4°C) and the total sampling and analysis speed. These results point towards a decrease in storage-induced metabolome alterations when using our MetaSAMP®s. Significant salivary and urinary metabolome alterations when storing crude biofluids at 4°C have been reported to occur after 6 hours (*60*) and 5 days (*14*), respectively, confirming our observations. The stabilizing properties of our optimized biofluid-specific MetaSAMP®s are hypothesized to result from the ad- and absorption capabilities of the electrospun fibrous network (*30*) and this both towards the different metabolites present in the biofluid and its aqueous content. In particular this water content present in the crude biofluids has been shown to provide a means for diverse degradation reactions (oxidation and hydrolysis) and microbial activity (enzymes) (*12*). In line herewith, the gastrointestinal matrices (feces and saliva) benefited most from the MetaSAMP®s stabilizing effects. Moreover, the MetaSAMP®s' protective PAN cover layer also provides a certain degree of shielding of the biofluid metabolites (small molecules) captured via chemical and/or physical interactions (Supplementary Fig. 11) and may hence contribute to this reduced degradation and transformation. Alternative AIMS-based techniques, including other LA-REIMS-based approaches (*1*, *17*), require relatively long collection procedures and/or sample preparation periods that take several hours up to days (*61*). The total analysis time of our optimized biofluid-specific MetaSAMP®-LA-REIMS methodology was <20 min per sample.

We successfully benchmarked the biofluid-specific MetaSAMP®s in the context of a clinically relevant application using samples from two pediatric cohorts (MetaBEAse and OPERA). The ever-increasing rise in overweight and obesity urges the development of cost-effective ways to screen for elevated metabolic risk as early as possible, when metabolic impairments are still reversible (*2*). Our findings provided evidence that MetaSAMP®-based metabotyping enables similarly to superior discriminative categorization of children based on weight classification compared to crude biofluid LA-REIMS analysis (*1*). This was confirmed by high predictive AUC values (>0.9), indicating good to excellent sensitivity and specificity of the metabolic fingerprints sampled and analyzed via MetaSAMP®-LA-REIMS analysis regarding weight classification. Moreover, the obtained metabolic fingerprints exhibited meaningful pathophysiological correlations with a whole range of relevant anthropometric and clinical parameters for (childhood) overweight and obesity. Indeed, the correlations found in this study showed similar (*62*, *63*) or improved (*53*, *63*) Spearman ρ-values (up to 0.5) compared to earlier work. For example, we observed a correlation between the fecal metabolome, BMI and blood lipid levels (Spearman ρ-values of up to 0.4), in line with previous results concerning the fecal metabolome of obese adults (*63*). Similarly, Spearman ρ-values of up to 0.3 for fecal microbiome diversity with BMI and glycemic and lipid measurements in adults were reported recently (*53*) reported, while our MetaSAMP®s reached ρ-values of up to 0.6 regarding glycemic measurements such as glucose and insulin. In accordance with the literature, we observed that acylcarnitines were positively correlated in children with IOTF>1 and with WC, WHR and systolic BP, inferring future metabolic risk(*2*). Furthermore, similar correlations between anthropometric measurements with 7-ketocholesterol were noted and of clinical relevance as cholesterol derivates are involved in macrophage foam cell formation and thus atherosclerosis (*2*). Finally, we successfully demonstrated the targeted application of our rectal MetaSAMP®-LA-REIMS approach of which the results indicated that potentially clinically relevant fecal metabolites may be detected with acceptable intra-assay and intermediate precision according to FDA recommendations (*55*).

Although the merits of AIMS have been confined to the agnostic nature of untargeted metabolomics with its proven broad clinical usefulness (*64*), there still is much to glean from the reproducibility and quantitation exquisiteness of state-of-the-art conventional chromatography-based analytical platforms (*16*). Further research is also warranted to longitudinally follow up large-scale cohorts of childhood overweight and obesity to consolidate the potential of MetaSAMP®-based metabotyping as a risk categorization tool in precision medicine. Herein, *ex vivo* and *in vivo* sampling using the MetaSAMP® should contribute to cross-validate results and to further reveal

potential predictive and prognostic value of differential marker molecules qualified with the aid of more dedicated hyphenated techniques.

Our biofluid-specific MetaSAMP®-LA-REIMS methodology provides a promising approach toward the first-line segregation of increased metabolic risk based on distinctive fingerprints that may overcome the limitations of conventional crude biofluid AIMS metabolomics analysis, such as matrix effects. Moreover, biofluid collection, transport and storage are substantially facilitated using our optimized biofluid-specific MetaSAMP®s while supporting the short-term metabolome stability, as such decreasing the possible loss of clinically relevant metabolites in the duration between the home/practitioner's office sampling and laboratory-scale analysis. Rapid high-throughput fingerprinting by MetaSAMP®-LA-REIMS may as such be installed as a prescreening approach, circumventing costly and cumbersome analyses prior to the further in-depth study of discriminative metabolites.

Materials and Methods

Experimental Design

Chemicals and Standards

IPA, methanol (MeOH), ethanol (EtOH), and ACN (all LC–MS-grade) were purchased from Fisher Scientific (UK). N,N-Dimethylformamide (DMF) and chloroform ($CHCl_3$) were purchased from EMPLURA Merck Millipore (Belgium) and Sigma Aldrich (USA), respectively. Ultrapure water (UPW) was obtained through a Sartorius Arium 661 UV water purification system (Millipore, Belgium). Analytical standards (3-hydroxybutyric acid, linoleic acid, L-carnosine, 1,2-dioleoyl-sn-glycero-3-phospho-rac-(1-glycerol) (DOPG), 1-palmitoyl-2-oleoyl-sn-glycero-3-(phospho-rac-(1-glycerol)) (POPG), D-mannitol, myo-inositol, L-cysteine, L-arginine, L-kynurenine and taurolitocholate-3-sulfate) and leucine enkephalin were purchased from Sigma–Aldrich (USA), ICN Biomedicals Inc. (USA), TLC Pharmchem (Canada), or Waters Corporation (Milford, MA). Information on the purchased polymers and preliminary evaluation of different polymer solutions is given under Supplementary Note 1.

Electrospinning

The polymers (PVP/PS) were loaded in a 20 mL syringe and fed through a syringe KD Scientific KDS-100-CE Pump Series 100 (Sigma Aldrich, USA) using a capillary 18G needle of 0.80 mm inner diameter at a flow rate of 1 mL h^{-1} and 1.5 mL min^{-1} for the core (PVP/PS for the salivary and rectal MetaSAMP® and PVP/PS-PAN for the urinary MetaSAMP®) and PAN cover

layers, respectively. A Glassman High Voltage Series EH (High Bridge, USA) was clamped to the tip of the needle and was used to apply a voltage between 15-17.5 kV. The tip-to-collector distance was averaged at 15 cm but slightly altered during the ES process towards attaining a stable, i.e., steady-state, Taylor cone (*65*). The nanofibrous network was collected on a grounded, thick Al foil-covered metal drum collector (Linari NanoTech, Italy) rotating at 125 RPM. All experiments were performed at ambient conditions, i.e., RT 22±2°C and RH 30±10%, in a fumehood (*65*). Modulated differential scanning calorimetry measurements were performed (Supplementary Fig. 3) to determine the Tg of the polymers in the blend. Specifications of the viscosity measurements, SEM analyses, modulated differential scanning calorimetry method and CAMs are elaborated under Supplementary Note 2.

LA-REIMS Instrumental Analysis

All LA-REIMS analyses were performed using our previously biofluid-specific optimized protocols (*1*), except for the rectal MetaSAMP®-LA-REIMS analysis for which the protocol was optimized as described in Supplementary Note 1. A mid-IR laser system (Opolette 2940, Opotek, Carlsbad, USA) was used as a desorption and ionization source hyphenated by a PTFE aerosol channeling tube to a Xevo G2-XS quadrupole time-of-flight (Q-ToF) mass spectrometer (Waters Corporation, Milford, MA). A brief description of the instrumental analysis is described under Supplementary Note 3. For all biofluid matrices, different solvents (MeOH, EtOH, IPA and CAN) and flow rates were investigated (Supplementary Note 3, Supplementary Fig. 12 and Supplementary Table 13), ranging from 150 to 300 µL min^{-1}.

Clinical Study Samples

Fresh feces (Fecotainer®, Excretas Medical BV, The Netherlands) and urine from children (6-12 years, Metabolomics research on Early Metabolic Disease (MetaBEAse) cohort) and saliva from children (6–16 years, Obesity Prevention through Emotion Regulation in Adolescents (OPERA) cohort (*41*)) were collected upon approval by the Ghent University Hospital Ethics Committee (BC-06939 and EC 2016/0673, respectively). The MetaBEAse cohort is also registered at ClinicalTrials.gov (NCT04632511). Samples were stored at -80°C following collection and thawed at RT 22±2°C before analysis. Participant fecal samples underwent lyophilization (Christ 1-4 Alpha LSC*plus*), resulting in an average removal of 55.9%±6.4% water. Saliva samples were

pretreated as described previously (*13*), and urine samples were used after thawing without additional processing.

The study participants were of both sexes (Table 1), were pseudonymized, and did not receive antibiotic treatment for at least three months before sample donation or take any long-term medication (*66*). The classification was performed based on BMI *z*-scores (adjusted BMI for age and sex) (*67*) and IOTF score (*68*).

Sample Preparation for Optimization and Short-term Stability Experiments

For initial optimization experiments with the rectal MetaSAMP®, rectal sampling was mimicked by impregnating pieces (1 cm x 1 cm) of the electrospun PVP/PS membranes with the contents of freshly collected porcine colon and rectum (EC2018_70 and EC2018_91, Ghent University, Department of Translational Physiology, Infectiology and Public Health, Merelbeke, BE). To optimize and evaluate the short-term stability of the rectal, salivary and urinary MetaSAMP®s nanofiber composition, remaining aliquots from the samples of our MetaBEAse and OPERA pediatric cohorts (n=6 for each biofluid) were combined to create pooled QC samples that aimed to reflect inherent biological variation. Pooled QC samples of the 3 biofluids were used to maximize metabolite coverage without substantially increasing the number of analyses (*12*, *69*).

For the pooled QC sample used during optimization and short-term stability experiments, fecal water was prepared by the addition of UPW to the fresh fecal sample at a 1:4 ratio (*w/v %*) followed by homogenization (Stomacher 400, Seward, Worthing, UK) for 10 min at the highest intensity(*70*) (see also Supplementary Note 3, Supplementary Fig. 13 and Supplementary Table 15) and subsequent centrifugation (Rotanta 460R, Hettich Zentrifugen, Tuttlingen, Germany) at RT (500 x *g*, 2 min). The collected supernatant was divided into aliquots, which were stored at -80°C. As such, freeze–thaw cycling, which may negatively affect metabolome stability(*12*), was limited since a new aliquot was used, after thorough vortexing (1 min at 400 x *g*, IKA vortex 3, IKA, Staufen, Germany), for every optimization experiment performed. A volume of 30 µL of fecal water, urine or saliva (*1*) was spiked onto an electrospun nanofibrous membrane piece of 1 x 1 cm in size, matching the dimensions of a 24-well plate (Greiner CELLSTAR, Greiner Bio One, Frickenhausen, Germany). Samples were allowed to extract for 10 min (impregnation time). For direct biofluid analysis (i.e., without MetaSAMP® impregnation), 100 µL of each sample was added to a 96-well plate (Greiner 96-well microplates, Greiner Bio One, Frickenhausen, Germany) in accordance with Plekhova (*1*).

Compositional Optimization and Short-term Stability Evaluation of the Biofluid-specific MetaSAMP®s

The ratios at which PVP and PS were blended were controlled by varying the relative weight ratios of each polymer as well as the polymer weight relative to the total solution weight (w/w). A statistical design of experiments was constructed with the software programs Modde™ (Sartorius, Germany) and JMP™ 12.0 (SAS Institute Inc., Cary, USA), whereby the compositions (polymer ratio (PVP%, *w/w*), polymer weight% (*w/w*)), duration of spinning the PAN cover layer (min) and duration of spinning the core membrane (h) were evaluated towards metabolome coverage, measurement repeatability (*n*=5) (*66*), summarized normalized LA-REIMS intensity(*71*) and quality of the fiber network by inspecting SEM images. Moreover, the addition of the PAN top layer (5-15%, w/w) was examined through the quality of the fiber network by SEM and evaluated in terms of metabolome coverage (Supplementary Tables 5 and 6). Subsequently, the number of molecular features covered and their relative number (%) with CV ≤30% (*66*) were compared.

A short-term stability study of the impregnated optimized rectal, salivary and urinary MetaSAMP®s was performed by using QC pool samples (see above) for up to 48h at RT 22±2°C and 4°C. As described above, biofluids were either applied on the respective MetaSAMP® surface or analyzed as such directly upon collection (first timepoint) and after storage (second time point). For each condition 8 sample aliquots were analyzed, of which 3 replicate measurements were performed.

Analytical and Biological Validation of the MetaSAMP®-LA-REIMS Methodology

The optimized MetaSAMP® configurations were subjected to analytical (targeted and untargeted) and biological (untargeted) validation. To this end, feces and urine from children (MetaBEAse cohort, *n*=88, IOTF≥1 and *n*=146, IOTF <1) and saliva samples from children (OPERA cohort (*41*), *n*=66, IOTF 0, *n*=29 IOTF≥1) (*13*) were impregnated under the same experimental conditions as described above onto the optimized electrospun membranes.

The instrumental, intra-assay precision or repeatability, and intermediate precision of the MetaSAMP®-LA-REIMS methodology was assessed to confirm the analytical method as fit-for-purpose according to FDA recommendations (*11, 55*). This is, technical repeatability was assessed by LA-REIMS automated analysis (*n*=3 burns of the same sample) (*1*) of the pooled QC samples and standard mixtures. For the intra-assay and intermediate precision tests, 5 pieces from an

electrospun membrane were analyzed under repeatable experimental conditions by the same operator, and this setup was used again on a different day by another operator, respectively.

The target analytes (30 µL at 100 ng μL^{-1}) were spiked using a micropipette onto the rectal MetaSAMP® membranes in neat solvent (UPW and isopropylacohol, according to logP of the target analytes) as well as in fecal water into a 24-well plate (Greiner CELLSTAR, Greiner Bio One, Frickenhausen, Germany, and subjected to our automatic platform for LA-REIMS analysis(*1*). The mass spectra generated in MassLynx™ and through our in-house data analysis pipeline as well as mass accuracy data for both platforms were investigated, and the repeatability of the targeted analysis was examined using the CV values. For this purpose, we evaluated the accurate *m/z* values of detectable adducts of the molecular ions to three decimal places after mass drift correction (LA-REIMS data and the monoisotopic mass from HMDB (*56*)).

To assess the applicability of the MetaSAMP®-LA-REIMS platform, the established methodology was implemented in the clinical context of pediatric overweight and obesity (see above). The associations between anthropometric and clinical and metabolic blood data with molecular features were computed in those two independent cohorts (MetaBEAse and OPERA (*41*) cohorts) using Spearman's rank correlation analysis (*53*) (absolute correlations reported with ρ) and corresponding FDR-adjusted *p* values (Wilcoxon rank-sum tests) for each pair of metadata and molecular feature under investigation.

Ultrahigh-performance liquid chromatography coupled to HRMS analysis, a more comprehensive analysis technique that is conventionally used in metabolomics research (Tiers 1-3 according to metabolite identification standards (*69*)), was addressed to enable metabolite annotation of potentially clinically relevant molecular features. For this purpose, a selection of representative crude stool patient samples (n=4, extracted stool samples, MetaBEAse cohort) and 525 fecal in-house analytical standards (Supplementary Table 8) were analyzed according by combined complementary metabolomics (*11*) and lipidomics (*66*) analysis.

For every validation experiment, a pool of randomly selected clinical cohort samples ($n \geq 20$) was prepared to include as QC sample during analysis to monitor instrument performance. For this purpose, QC samples were included at the beginning and end of the analytical batch (n=6), as well as during analysis (n=2) after every 10 samples, and samples were analyzed in a randomized order.

Data and Statistical Analysis

LA-REIMS molecular fingerprints were acquired by MassLynx™ (version 4.2, Waters, Corporation, Milford, MA, stored as raw directories). To counteract plausible time-dependent

instrumental variability, lock mass correction against the *m/z* value of leucine enkephalin (554.262 Da for negative ion mode data) was performed and preprocessed using Progenesis® Bridge (version 1.0.29) and QI (version 2.3., Waters Corporation, Milford, MA), as described previously (*1*). Further data analyses were conducted using R (version 3.4.3, Vienna, Austria) and Python (version 3.7.4, Fredericksburg, VA, USA) (Supplementary Table 14). Preprocessed data were subjected to pretreatment optimization, including a range of tested normalization strategies, which included quality control-based robust locally estimated scatterplot smoothing signal correction (QC-RLSC algorithm) (*13*), internal QC correction, and total ion current (TIC) correction as well as their combinations. Molecular features, as addressed in terms of feature count and % of features below CV threshold, were assigned as relevant only when they occurred in at least 80% of QC replicates. For intensity analysis and the evaluation of replicate measures, mean, SD and CV values were calculated. All multivariate models were built using SIMCA® (Sartorius, Göttingen, Duitsland) after selection of the best raw data pretreatment strategy and the associated data. Unsupervised principal component analysis (PCA) was used for the identification of outliers, the evaluation of instrument stability based on QC clustering, and the assessment of the natural patterning of samples according to inherent metabolic fingerprints. Supervised multivariate statistical modeling using OPLS-DA was performed to assess the discriminative and predictive performance of the metabolic fingerprints. Additionally, ROC analysis of the fecal and urinary metabolome coverage (MetaBEAse cohort) was executed based on the logistic regression classification model (75-25 train-test split after balancing data, performed using five-fold cross-validation). Logistic regression is a popular method to analyze injury case-control studies, and has some advantages over linear regression analysis, using maximum likelihood estimation methods. To optimize the predictive power of our models, molecular features (1750 in total) were iteratively eliminated from the dataset while monitoring the accuracy of models trained on this reduced dataset. Quantification of AUC values and corresponding 95% CI was performed using bootstrap resampling (n=200). To perform the Spearman correlation analysis, normalized, log-transformed and Pareto scaled datasets were used. In addition, univariate Wilcoxon rank-sum tests with continuity correction were performed with the normalized dataset (rectal MetaSAMP®) to study which molecular features showed good and significant (p<0.05) correlations with anthropometric and/or clinical parameters. Targeted data processing of the significant molecular features was carried out with Xcalibur™ 3.0 software (Thermo Fisher Scientific, USA), whereby compounds were identified based on their *m/z* value, C-isotope profile, and retention time relative to that of the internal standard, followed by putative identification (*69*) of significant and highly correlated LA-REIMS-MetaSAMP® features (mass deviation below 50 ppm). Pairwise univariate and multiple comparisons were evaluated for the

identified molecular features according to different IOTF groups based on Wilcoxon rank-sum test with continuity correction and Kruskal–Wallis test with Dunn's post-hoc test, respectively.

The R language was also used for preprocessing, data handling, and statistical analysis of data from the targeted analysis of spiked analytes representing clinically relevant metabolites in (childhood) overweight and obesity (*2*) with varying physicochemical properties (mass error tolerance set at a maximum value of 150 ppm), including a visualization tool generating mass spectra and graphics (Supplementary Table 10).

References

1. V. Plekhova, L. Van Meulebroek, M. De Graeve, A. Perdones-montero, M. De Spiegeleer, E. De Paepe, E. Van De Walle, Z. Takats, S. J. S. Cameron, L. Vanhaecke, Rapid ex vivo molecular fingerprinting of biofluids using laser-assisted rapid evaporative ionization mass spectrometry. *Nat. Protoc.*, doi:10.1038/s41596-021-00580-8.
2. M. De Spiegeleer, E. De Paepe, L. Van Meulebroek, I. Gies, J. De Schepper, L. Vanhaecke, Paediatric obesity: a systematic review and pathway mapping of metabolic alterations underlying early disease processes. *Mol. Med.* **27** (2021), doi:10.1186/s10020-021-00394-0.
3. G. F. Giskeodegard, S. K. Davies, V. L. Revell, H. Keun, D. J. Skene, Diurnal rhythms in the human urine metabolome during sleep and total sleep deprivation. *Sci. Rep.* **5**, 14843 (2015).
4. M. McEniry, Early-life conditions and older adult health in low- and middle-income countries: A review. *J. Dev. Orig. Health Dis.* **4**, 10–29 (2013).
5. N. Liu, J. Xiao, C. Gijavanekar, K. L. Pappan, K. E. Glinton, B. J. Shayota, A. D. Kennedy, Q. Sun, V. R. Sutton, S. H. Elsea, Comparison of Untargeted Metabolomic Profiling vs Traditional Metabolic Screening to Identify Inborn Errors of Metabolism. *JAMA Netw. Open*. **4**, 1–14 (2021).
6. World Health Organization, *Who European Regional Obesity Report 2022* (2022; http://apps.who.int/bookorders.).
7. R. L. Rosenfield, CLINICAL REVIEW: Identifying Children at Risk for Polycystic Ovary Syndrome (2007), doi:10.1210/jc.2006-2012.
8. P. M., C. C., G. R.L., S. B., H. C.M., Y. G., J. J.E., S. C.B., L. A.P., D. B.T., A. A.P., Diabetes and prediabetes are significantly higher in morbidly obese children compared with obese children. *Endocr. Pract.* **21**, 1046–1053 (2015).
9. A. Deeb, S. Attia, S. Mahmoud, G. Elhaj, A. Elfatih, Dyslipidemia and Fatty Liver Disease in Overweight and Obese Children. *J. Obes.* **2018**, 8626818 (2018).
10. D. C. Masquio, A. eP. Ganen, R. M. Campos, P. eL. Sanches, F. C. Corgosinho, D. Caranti, L. Tock, M. T. de Mello, S. Tufik, A. R. Dâmaso, Cut-off values of waist circumference to predict metabolic syndrome in obese adolescents. *Nutr. Hosp.* **31**, 1540–1550 (2015).
11. E. De Paepe, L. Van Meulebroek, C. Rombouts, S. Huysman, K. Verplanken, B. Lapauw, J. Wauters, L. Y. Hemeryck, L. Vanhaecke, A validated multi-matrix platform for metabolomic fingerprinting of human urine, feces and plasma using ultra-high performance liquid-chromatography coupled to hybrid orbitrap high-resolution mass spectrometry. *Anal. Chim. Acta*. **1033**, 108–118 (2018).
12. M. De Spiegeleer, M. De Graeve, S. Huysman, A. Vanderbeke, L. Van Meulebroek, L.

Vanhaecke, Impact of storage conditions on the human stool metabolome and lipidome : Preserving the most accurate fingerprint. *Anal. Chim. Acta*. **1108** (2020).
13. K. Wijnant, L. Van Meulebroek, B. Pomian, K. De Windt, S. De Henauw, N. Michels, L. Vanhaecke, Validated Ultra-High-Performance Liquid Chromatography Hybrid High-Resolution Mass Spectrometry and Laser-Assisted Rapid Evaporative Ionization Mass Spectrometry for Salivary Metabolomics (2020), doi:10.1021/acs.analchem.9b05598.
14. J. Laparre, Z. Kaabia, M. Mooney, T. Buckley, M. Sherry, B. Le Bizec, G. Dervilly-Pinel, Impact of storage conditions on the urinary metabolomics fingerprint. *Anal. Chim. Acta*. **951**, 99–107 (2016).
15. W. Lu, X. Su, M. S. Klein, I. A. Lewis, O. Fiehn, J. D. Rabinowitz, Metabolite Measurement: Pitfalls to Avoid and Practices to Follow (2017), doi:10.1146/annurev-biochem.
16. L. Van Meulebroek, S. Cameron, V. Plekhova, M. De Spiegeleer, K. Wijnant, N. Michels, S. De Henauw, B. Lapauw, L. Vanhaecke, Rapid LA-REIMS and comprehensive UHPLC-HRMS for metabolic phenotyping of feces. *Talanta*, 121043 (2020).
17. P. Pruski, D. A. MacIntyre, H. V. Lewis, P. Inglese, G. D. S. Correia, T. T. Hansel, P. R. Bennett, E. Holmes, Z. Takats, Medical Swab Analysis Using Desorption Electrospray Ionization Mass Spectrometry: A Noninvasive Approach for Mucosal Diagnostics. *Anal. Chem.* **89**, 1540–1550 (2017).
18. S. J. S. Cameron, J. L. Alexander, F. Bolt, A. Burke, H. Ashrafian, J. Teare, J. R. Marchesi, J. Kinross, J. V. Li, Z. Takáts, Evaluation of Direct from Sample Metabolomics of Human Feces Using Rapid Evaporative Ionization Mass Spectrometry. *Anal. Chem.* (2019), doi:10.1021/acs.analchem.9b02358.
19. X. Li, R. Xu, X. Wei, H. Hu, S. Zhao, Y. M. Liu, Direct Analysis of Biofluids by Mass Spectrometry with Microfluidic Voltage-Assisted Liquid Desorption Electrospray Ionization. *Anal. Chem.* **89**, 12014–12022 (2017).
20. B. Fatou, P. Saudemont, E. Leblanc, D. Vinatier, V. Mesdag, M. Wisztorski, C. Focsa, M. Salzet, M. Ziskind, I. Fournier, In vivo Real-Time Mass Spectrometry for Guided Surgery Application. *Sci. Rep.* **6**, 1–14 (2016).
21. N. Abbassi-Ghadi, E. A. Jones, M. Gomez-Romero, O. Golf, S. Kumar, J. Huang, H. Kudo, R. D. Goldin, G. B. Hanna, Z. Takats, A Comparison of DESI-MS and LC-MS for the Lipidomic Profiling of Human Cancer Tissue. *J. Am. Soc. Mass Spectrom.* **27**, 255–264 (2016).
22. A. Alonso, S. Marsal, A. JuliÃ, Analytical Methods in Untargeted Metabolomics: State of the Art in 2015. *Front. Bioeng. Biotechnol.* **3**, 1–20 (2015).
23. T. H. Kuo, E. P. Dutkiewicz, J. Pei, C. C. Hsu, Ambient Ionization Mass Spectrometry Today and Tomorrow: Embracing Challenges and Opportunities. *Anal. Chem.* **92**, 2353–2363 (2020).
24. J. Geltmeyer, L. Van Der Schueren, F. Goethals, K. De Buysser, K. De Clerck, Optimum sol viscosity for stable electrospinning of silica nanofibres. *J. Sol-Gel Sci. Technol.* **67**, 188–195 (2013).
25. M. S. Islam, B. C. Ang, A. Andriyana, A. M. Afifi, A review on fabrication of nanofibers via electrospinning and their applications. *SN Appl. Sci.* **1**, 1–16 (2019).
26. N. Reyes-Garcés, E. Gionfriddo, G. A. Gómez-Ríos, M. N. Alam, E. Boyacl, B. Bojko, V. Singh, J. Grandy, J. Pawliszyn, Advances in Solid Phase Microextraction and Perspective on Future Directions. *Anal. Chem.* **90**, 302–360 (2018).
27. T. Lu, S. V Olesik, Electrospun Nanofibers as Substrates for Surface-Assisted Laser Desorption/Ionization and Matrix-Enhanced Surface-Assisted Laser Desorption/Ionization Mass Spectrometry (2013).
28. E. Gionfriddo, E. Boyacl, J. Pawliszyn, New Generation of Solid-Phase Microextraction

Coatings for Complementary Separation Approaches: A Step toward Comprehensive Metabolomics and Multiresidue Analyses in Complex Matrices. *Anal. Chem.* **89**, 4046–4054 (2017).
29. B. Onat, H. Rosales-Solano, J. Pawliszyn, Development of a Biocompatible Solid Phase Microextraction Thin Film Coating for the Sampling and Enrichment of Peptides. *Anal. Chem.* **92**, 9379–9388 (2020).
30. T. Meireman, L. Daelemans, S. Rijckaert, H. Rahier, W. Van Paepegem, K. De Clerck, Delamination resistant composites by interleaving bio-based long-chain polyamide nanofibers through optimal control of fiber diameter and fiber morphology. *Compos. Sci. Technol.* **193**, 108126 (2020).
31. K. L. Nielsen, M. L. Hartvigsen, M. S. Hedemann, H. N. Lræke, K. Hermansen, K. E. Bach Knudsen, Similar metabolic responses in pigs and humans to breads with different contents and compositions of dietary fibers: A metabolomics study. *Am. J. Clin. Nutr.* **99**, 941–949 (2014).
32. S. Huysman, F. Vanryckeghem, E. De Paepe, F. Smedes, S. A. Haughey, C. T. Elliott, K. Demeestere, L. Vanhaecke, Hydrophilic Divinylbenzene for Equilibrium Sorption of Emerging Organic Contaminants in Aquatic Matrices. *Environ. Sci. Technol.* **53**, 10803–10812 (2019).
33. P. Franco, I. De Marco, The Use of Poly(N-vinyl pyrrolidone) in the Delivery of Drugs: A Review. *Polymers (Basel).* (2020), doi:10.3390/polym12051114.
34. X. Liu, T. Lin, J. Fang, G. Yao, H. Zhao, M. Dodson, X. Wang, In vivo wound healing and antibacterial performances of electrospun nanofibre membranes (2010), doi:10.1002/jbm.a.32718.
35. J. Xue, T. Wu, Y. Dai, Y. Xia, Electrospinning and electrospun nanofibers: Methods, materials, and applications. *Chem. Rev.* **119** (2019), pp. 5298–5415.
36. J. Niska-Blakie, L. Gopinathan, K. N. Low, Y. L. Kien, C. M. F. Goh, M. J. Caldez, E. Pfeiffenberger, O. S. Jones, C. B. Ong, I. V Kurochkin, V. Coppola, L. Tessarollo, H. Choi, Y. Kanagasundaram, F. Eisenhaber, S. Maurer-Stroh, P. Kaldis, Knockout of the non-essential gene SUGCT creates diet-linked, age-related microbiome disbalance with a diabetes-like metabolic syndrome phenotype. *Cell. Mol. Life Sci.* (2019), doi:10.1007/s00018-019-03359-z.
37. M. Reyman, M. A. van Houten, K. Arp, E. A. M. Sanders, D. Bogaert, Rectal swabs are a reliable proxy for faecal samples in infant gut microbiota research based on 16S-rRNA sequencing. *Sci. Rep.* **9**, 1–8 (2019).
38. R. B. Jones, X. Zhu, E. Moan, H. J. Murff, R. M. Ness, D. L. Seidner, S. Sun, C. Yu, Q. Dai, A. A. Fodor, M. A. Azcarate-Peril, M. J. Shrubsole, Inter-niche and inter-individual variation in gut microbial community assessment using stool, rectal swab, and mucosal samples. *Sci. Rep.* **8**, 1–12 (2018).
39. E. A. Jones, D. Simon, T. Karancsi, J. Balog, S. D. Pringle, Z. Takats, Matrix assisted rapid evaporative ionization mass spectrometry. *Anal. Chem.* **91**, 9784–9791 (2019).
40. P. T. Ivanova, S. B. Milne, H. A. Brown, Identification of atypical ether-linked glycerophospholipid species in macrophages by mass spectrometry. *J. Lipid Res.* **51**, 1581–1590 (2010).
41. K. Wijnant, J. Klosowska, C. Braet, S. Verbeken, S. De Henauw, L. Vanhaecke, N. Michels, J.-B. Bouillon-Minois, Stress Responsiveness and Emotional Eating Depend on Youngsters' Chronic Stress Level and Overweight Academic Editors: Frederic Dutheil (2021), doi:10.3390/nu13103654.
42. I. Agueusop, P. B. Musholt, B. Klaus, K. Hightower, A. Kannt, Short-term variability of the human serum metabolome depending on nutritional and metabolic health status. *Sci. Rep.* **10**, 1–13 (2020).

43. E. De Paepe, L. Van Gijseghem, M. De Spiegeleer, E. Cox, L. Vanhaecke, A Systematic Review of Metabolic Alterations Underlying IgE-Mediated Food Allergy in Children. *Mol. Nutr. Food Res.* **2100536**, 1–12 (2021).
44. J. D. Blume, Bounding Sample Size Projections for the Area Under a ROC Curve, doi:10.1016/j.jspi.2007.09.015.
45. E. Chavira-Suarez, C. Rosel-Pech, E. Polo-Oteyza, M. Ancira-Moreno, I. Ibarra-Gonzalez, M. Vela-Amieva, N. Meraz-Cruz, C. Aguilar-Salinas, F. Vadillo-Ortega, Simultaneous evaluation of metabolomic and inflammatory biomarkers in children with different body mass index (BMI) and waist-to-height ratio (WHtR). *PLoS One*. **15** (2020), doi:10.1371/journal.pone.0237917.
46. P. Schober, L. A. Schwarte, Correlation coefficients: Appropriate use and interpretation. *Anesth. Analg.* **126**, 1763–1768 (2018).
47. American diabetes association, 2. Classification and diagnosis of diabetes: Standards of medical care in diabetesd2019. *Diabetes Care*. **42**, S13–S28 (2019).
48. M. Ramon-Krauel, M. J. Leal-Witt, Ó. Osorio-Conles, M. Amat-Bou, C. Lerin, D. M. Selva, Relationship between adiponectin, TNFα, and SHBG in prepubertal children with obesity. *Mol. Cell. Pediatr.* **8** (2021), doi:10.1186/S40348-021-00113-Z.
49. R. Santos-Silva, M. Fontoura, J. T. Guimarães, H. Barros, A. C. Santos, Association of dehydroepiandrosterone sulfate, birth size, adiposity and cardiometabolic risk factors in 7-year-old children. *Pediatr. Res.* (2021), doi:10.1038/s41390-021-01706-0.
50. M. D. Klok, S. Jakobsdottir, M. L. Drent, The role of leptin and ghrelin in the regulation of food intake and body weight in humans: a review. *Obes. Rev.* (2006), doi:10.1111/j.1467-789X.2006.00270.x.
51. A.-V. S.-T. T˘aut, A. Cozma, A. Fodor, S.-C. Coste, O. H. Orasan, V. Negrean, D. Pop, D.-A. S.-T. T˘aut, M. Grau, J. Lu, New Insights on the Relationship between Leptin, Ghrelin, and Leptin/Ghrelin Ratio Enforced by Body Mass Index in Obesity and Diabetes (2021), doi:10.3390/biomedicines9111657.
52. R. Liu, J. Hong, X. Xu, Q. Feng, D. Zhang, Y. Gu, J. Shi, S. Zhao, W. Liu, X. Wang, H. Xia, Z. Liu, B. Cui, P. Liang, L. Xi, J. Jin, X. Ying, X. Wang, X. Zhao, W. Li, H. Jia, Z. Lan, F. Li, R. Wang, Y. Sun, M. Yang, Y. Shen, Z. Jie, J. Li, X. Chen, H. Zhong, H. Xie, Y. Zhang, W. Gu, X. Deng, B. Shen, X. Xu, H. Yang, G. Xu, Y. Bi, S. Lai, J. Wang, L. Qi, L. Madsen, J. Wang, G. Ning, K. Kristiansen, W. Wang, Gut microbiome and serum metabolome alterations in obesity and after weight-loss intervention. *Nat. Med.* **23**, 859–868 (2017).
53. F. Asnicar, A. T. Chan, C. Huttenhower, T. D. Spector, N. Segata, S. E. Berry, A. M. Valdes, L. H. Nguyen, G. Piccinno, D. A. Drew, E. Leeming, R. Gibson, C. Le Roy, H. Al Khatib, L. Francis, M. Mazidi, O. Mompeo, M. Valles-Colomer, A. Tett, F. Beghini, L. Dubois, D. Bazzani, A. Maltez Thomas, C. Mirzayi, A. Khleborodova, S. Oh, R. Hine, C. Bonnett, J. Capdevila, S. Danzanvilliers, F. Giordano, L. Geistlinger, L. Waldron, R. Davies, G. Hadjigeorgiou, J. Wolf, J. M. Ordovás, Microbiome connections with host metabolism and habitual diet from 1,098 deeply phenotyped individuals. *Nat. Med.* **27**, 321–332 (2021).
54. M. Mar Rodríguez, D. Pérez, F. J. Chaves, E. Esteve, P. Marin-Garcia, G. Xifra, J. Vendrell, M. Jové, R. Pamplona, W. Ricart, M. Portero-Otin, M. R. Chacón, J. Manuel Fernández Real, Obesity changes the human gut mycobiome. *Sci. reportsts*. **5** (2015), doi:10.1038/srep14600.
55. Food and Drug Administration (FDA), Guidance for Industry: Bioanalytical Method Validation (2018) (available at https://www.fda.gov/downloads/drugs/guidances/ucm070107.Pdf).
56. D. S. Wishart, A. Guo, E. Oler, F. Wang, A. Anjum, H. Peters, R. Dizon, Z. Sayeeda, S.

Tian, B. L. Lee, M. Berjanskii, R. Mah, M. Yamamoto, J. Jovel, C. Torres-Calzada, M. Hiebert-Giesbrecht, V. W. Lui, D. Varshavi, D. Varshavi, D. Allen, D. Arndt, N. Khetarpal, A. Sivakumaran, K. Harford, S. Sanford, K. Yee, X. Cao, Z. Budinski, J. Liigand, L. Zhang, J. Zheng, R. Mandal, N. Karu, M. Dambrova, H. B. Schï Oth, R. Greiner, V. Gautam, HMDB 5.0: the Human Metabolome Database for 2022. *Nucleic Acids Res.* **50** (2022), doi:10.1093/nar/gkab1062.

57. J. Bian, S. V. Olesik, Surface-assisted laser desorption/ionization time-of-flight mass spectrometry of small drug molecules and high molecular weight synthetic/biological polymers using electrospun composite nanofibers. *Analyst*. **142**, 1125–1132 (2017).
58. S. Bouatra, F. Aziar, A. Mandal, R, Chi Guo, R. M. Wilson, The Human Urine Metabolome. *PLoS One*. **8** (2013).
59. Tipthara Phornpimon, T. Visith, *Chapter 7: Urinary Lipidomics* (2018), vol. 277.
60. D. Duarte, B. Castro, J. Pereira, J. Marques, A. Costa, A. Gil, "Evaluation of Saliva Stability for NMR Metabolomics: Collection and Handling Protocols" in *METABOLITES* (2020).
61. T. Vasiljevic, G. A. Gómez-Ríos, J. Pawliszyn, Single-Use Poly(etheretherketone) Solid-Phase Microextraction-Transmission Mode Devices for Rapid Screening and Quantitation of Drugs of Abuse in Oral Fluid and Urine via Direct Analysis in Real-Time Tandem Mass Spectrometry. *Anal. Chem.* **90**, 952–960 (2018).
62. S. Liang, Z. Hou, X. Li, J. Wang, L. Cai, R. Zhang, J. Li, The fecal metabolome is associated with gestational diabetes mellitus. *RSC Adv.* **9**, 29973–29979 (2019).
63. M. Cui, A. Trimigno, J. L. Castro-Mejía, S. Reitelseder, J. Bülow, R. L. Bechshøft, D. S. Nielsen, L. Holm, S. B. Engelsen, B. Khakimov, Human fecal metabolome reflects differences in body mass index, physical fitness, and blood lipoproteins in healthy older adults. *Metabolites*. **11**, 1–16 (2021).
64. J. D. Odom, R. V. Sutton, Metabolomics in Clinical Practice: Improving Diagnosis and Informing Management. *Clin. Chem.* **12**, 1–12 (2021).
65. G. Darko, A. Goethals, N. Torto, K. De Clerck, Steady state electrospinning of uniform polyethersulfone nanofibers using a non-heated solvent mixture. *Appl. Nanosci.* **6**, 837–845 (2016).
66. L. Van Meulebroek, E. De Paepe, V. Vercruysse, B. Pomian, S. Bos, B. Lapauw, L. Vanhaecke, Holistic Lipidomics of the Human Gut Phenotype Using Validated Ultra-High-Performance Liquid Chromatography Coupled to Hybrid Orbitrap Mass Spectrometry. *Anal. Chem.* **89**, 12502–12510 (2017).
67. M. Roelants, R. Hauspie, K. Hoppenbrouwers, References for growth and pubertal development from birth to 21 years in Flanders, Belgium. *Ann. Hum. Biol.* **36**, 680–694 (2009).
68. T. J. Cole, Extended international (IOTF) body mass index cut-offs for thinness, overweight and obesity. *Pediatr. Obes.* **7**, 284–294 (2012).
69. L. W. Sumner, A. Amberg, D. Barrett, M. H. Beale, R. Beger, C. A. Daykin, T. W. M. Fan, O. Fiehn, R. Goodacre, J. L. Griffin, T. Hankemeier, N. Hardy, J. Harnly, R. Higashi, J. Kopka, A. N. Lane, J. C. Lindon, P. Marriott, A. W. Nicholls, M. D. Reily, J. J. Thaden, M. R. Viant, Proposed minimum reporting standards for chemical analysis: Chemical Analysis Working Group (CAWG) Metabolomics Standards Initiative (MSI). *Metabolomics*. **3**, 211–221 (2007).
70. D. Monleón, J. M. Morales, A. Barrasa, J. A. López, C. Vázquez, B. Celda, Metabolite profiling of fecal water extracts from human colorectal cancer. *NMR Biomed.* **22**, 342–348 (2009).
71. S. Huysman, L. Van Meulebroek, F. Vanryckeghem, H. Van Langenhove, K. Demeestere, L. Vanhaecke, Development and validation of an ultra-high performance liquid

chromatographic high resolution Q-Orbitrap mass spectrometric method for the simultaneous determination of steroidal endocrine disrupting compounds in aquatic matrices. *Anal. Chim. Acta*. **984**, 140–150 (2017).

Acknowledgments

The Laboratory of Integrative Metabolomics (LIMET) research group is part of the Ghent University expertise center MSsmall. The colonic and rectal mucosa of slaughtered piglets was provided through the Laboratory of Virology (Faculty of Veterinary Medicine, Ghent University, Prof. Nauwynck). Regarding the recruitment of children with overweight and obesity, diverse hospitals and associated pediatricians, specifically UZ Antwerpen (Dr. Van De Maele and Dr. Vermeiren), UZ Brussel (Prof. De Scheper and Prof. Gies), UZ Leuven (Prof. Casteels, Dr. Jacobs and Dr. Rochtus), AZ Jan-Palfijn (Dr. Baeck), AZ Alma (Dr. Vanneste), AZ Sint-Lucas (Dr. Deman), AZ Sint-Jan Brugge (Dr. Depoorter) and OLV van Lourdes Waregem (Dr. De Lille), deserve our sincere gratitude. The authors also gratefully acknowledge Salma Kasim, who helped during the experimental work using our LA-REIMS platform.

Funding

FWO grant 1S57922N (MDS)

FWO grant 1192622N (KW)

ERC FWO Runner-up grant G0G0119N (LV, MDG)

BOF GOA grant 2017/000102 (KW, NM, SDH and LV)

BOF grant 01J07519 (LV, VP)

FWO Hercules grant AUG/17/09 (LV)

Author contributions

Conceptualization: MDS, KDC and LV

Methodology: MDS, VP, JG, ES, BP, VS, KDW and LV

Investigation: MDS, KW and ADL

Visualization: MDS, VPa, MDG and LV

Supervision: IG, NM, SDH, KDC and LV

Writing-original draft: MDS and LV

Writing-review & editing: MDS, MDG and LV

Competing Interests

All authors declare they have no competing interests.

Data and materials availability

The data supporting the findings from this study are available in the main text or the supplementary materials. Any remaining raw data and/or code data will be made available by the corresponding author upon reasonable request.

Figures and Tables

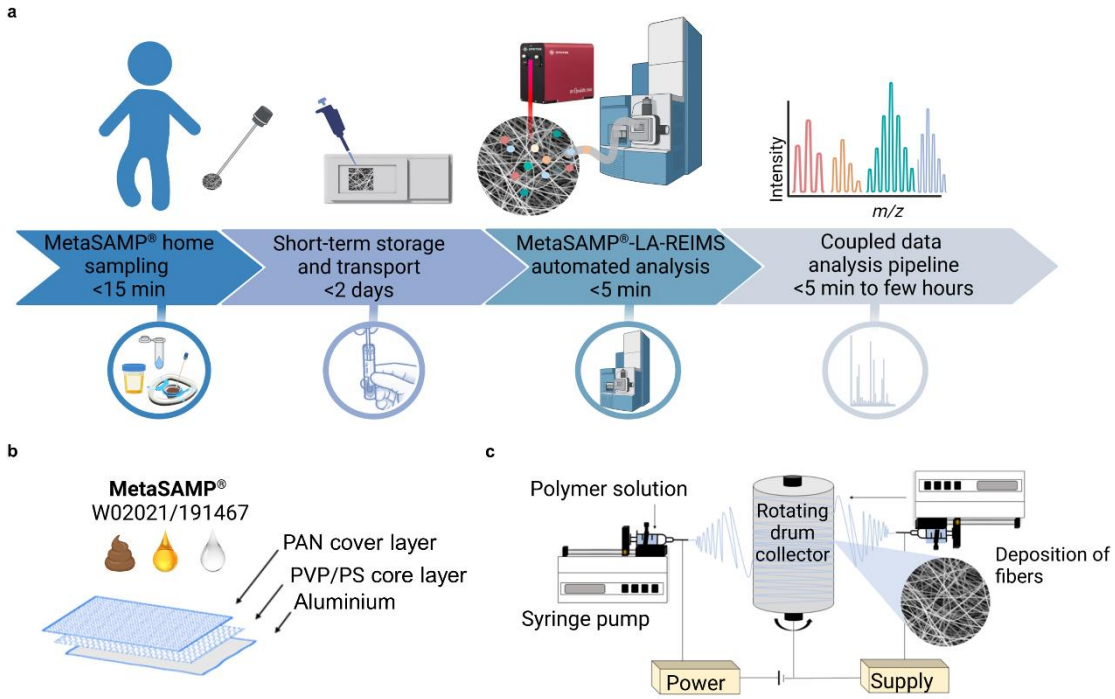

Figure 1. MetaSAMP®-LA-REIMS enables direct rectal, salivary and urinary metabotyping.

(A) A straightforward workflow for MetaSAMP® sampling hyphenated with LA-REIMS analysis. The analytes captured by MetaSAMP® (as a swab and/or kit configuration) are desorbed, and the resulting analyte-rich aerosol is directly transferred through a vent line to the inlet capillary, where subsequent quadrupole time-of-flight analysis takes place. Data are visualized in real-time through MassLynx™ software or an in-house data analysis pipeline across the mass range installed, i.e., 50 to 1200 *m/z* range, after which metabolomic alterations can be quickly revealed by multivariate data analysis, leading to first-line segregation and risk classification based on distinctive fingerprints for decision making in healthcare. (**B)** The 3-layered MetaSAMP® consists of a PAN cover layer, a PVP/PS core membrane, and an aluminium support layer as adhering electrically conductive collector. (**C)** The electrospinning setup

consists of a single-nozzle system that is duplicated to enable bidirectional electrospinning of the loaded polymer blends onto a continuously rotating drum.

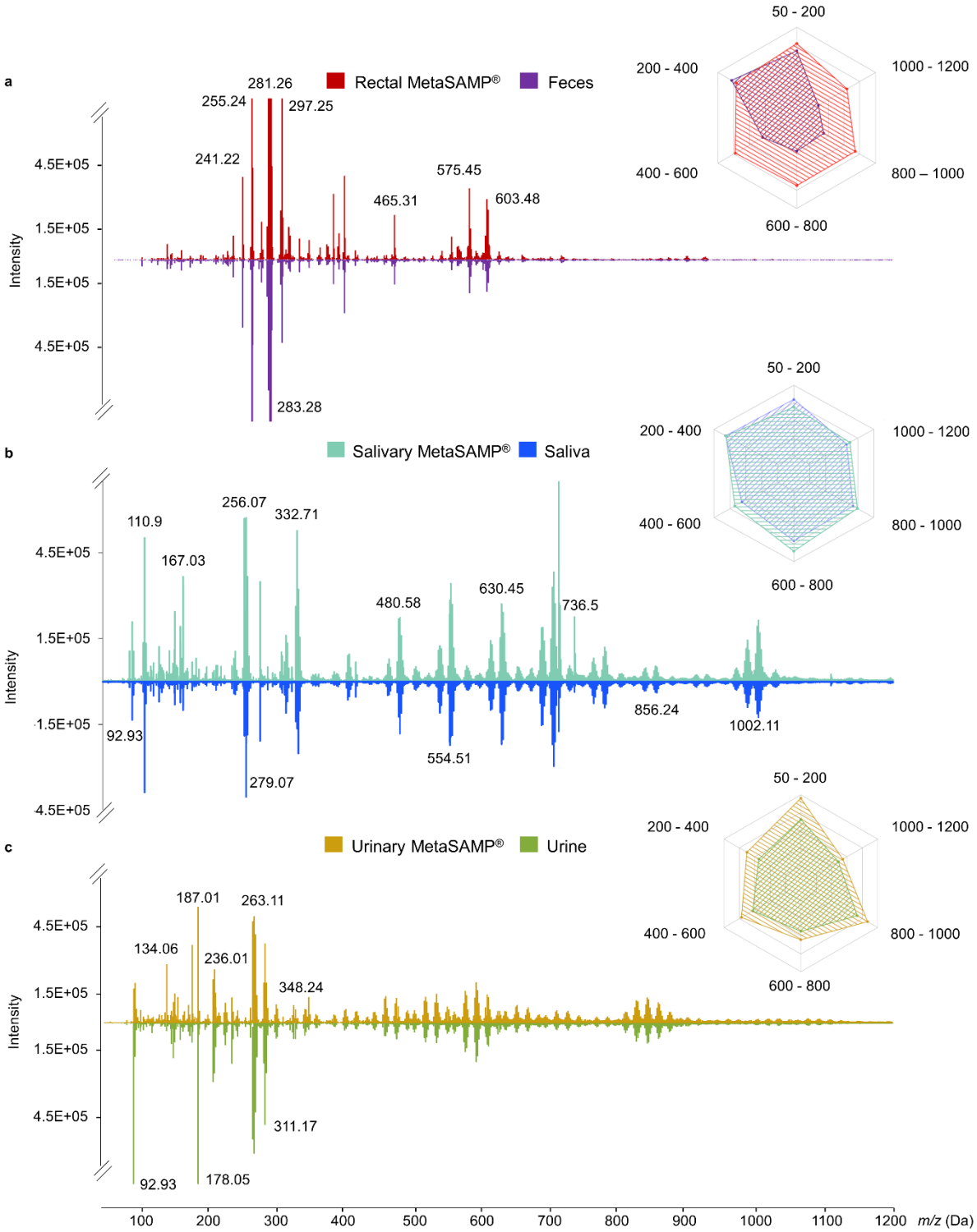

Figure 2. The use of MetaSAMPs® increases the richness and intensity of fecal, salivary and urinary metabolic fingerprints compared to those obtained with crude biofluid LA-REIMS-based metabotyping.

Head-to-tail comparison of LA-REIMS spectra obtained from impregnated **(A)** rectal, **(B)** salivary and **(C)** urinary MetaSAMPs® and feces, saliva and urine, respectively, measured in negative polarity mode (*m/z* range of 50–1200 Da depicted). The selected mirrored mass spectra are representative of the biofluid metabolomes of a child and adolescent with obesity (MetaBEAse cohort for the rectal and urinary and OPERA cohort (*41*) for the salivary MetaSAMP®s). Accompanying the mass spectra, radar charts visualized metabolome coverage of the crude biofluids (pooled QC samples originating from control children, *n*=3) and their corresponding optimized biofluid-specific MetaSAMP®.

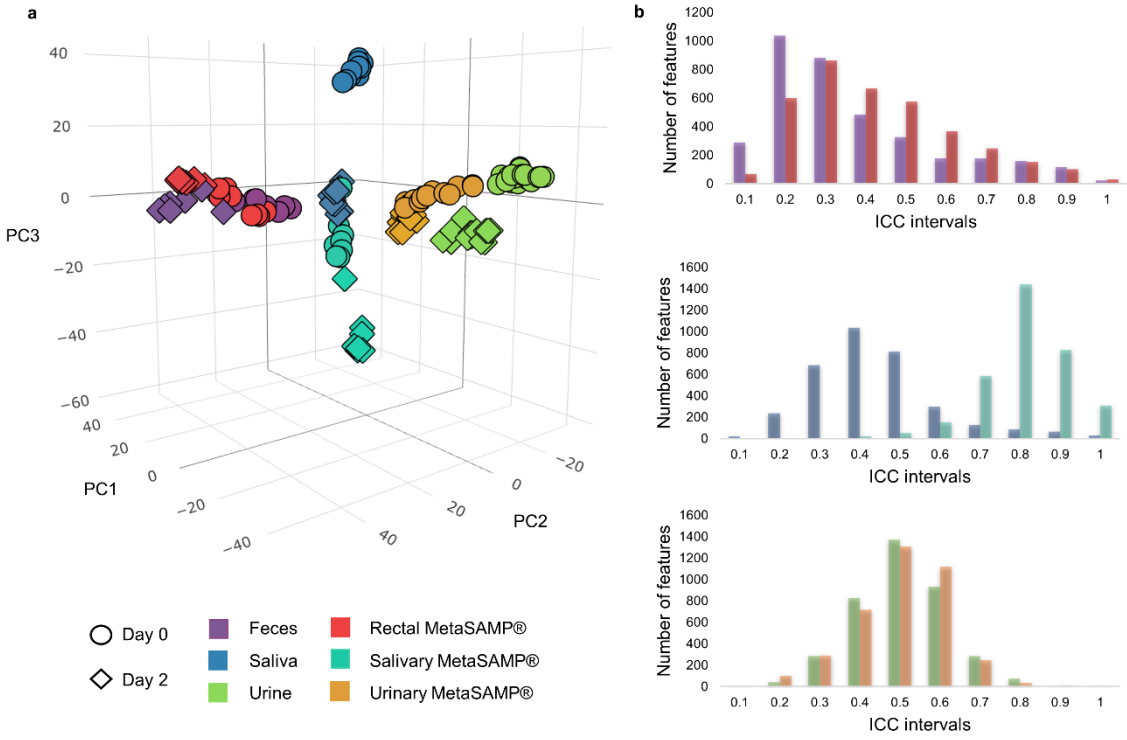

Figure 3. MetaSAMPs® improve short-term (48h) biofluid-specific metabolome stability as compared to crude biofluid analysis.

(A) 3D-PCA score plots presenting metabolome fluctuations upon storage at 4°C (day 0 versus day 2). The molecular feature count per ICC interval of pooled QC **(B)** fecal, saliva and urine samples, and the corresponding impregnated MetaSAMP®s (*n*=6 per biofluid) analyzed via LA-REIMS are depicted via histograms upon short-term storage at 4°C.

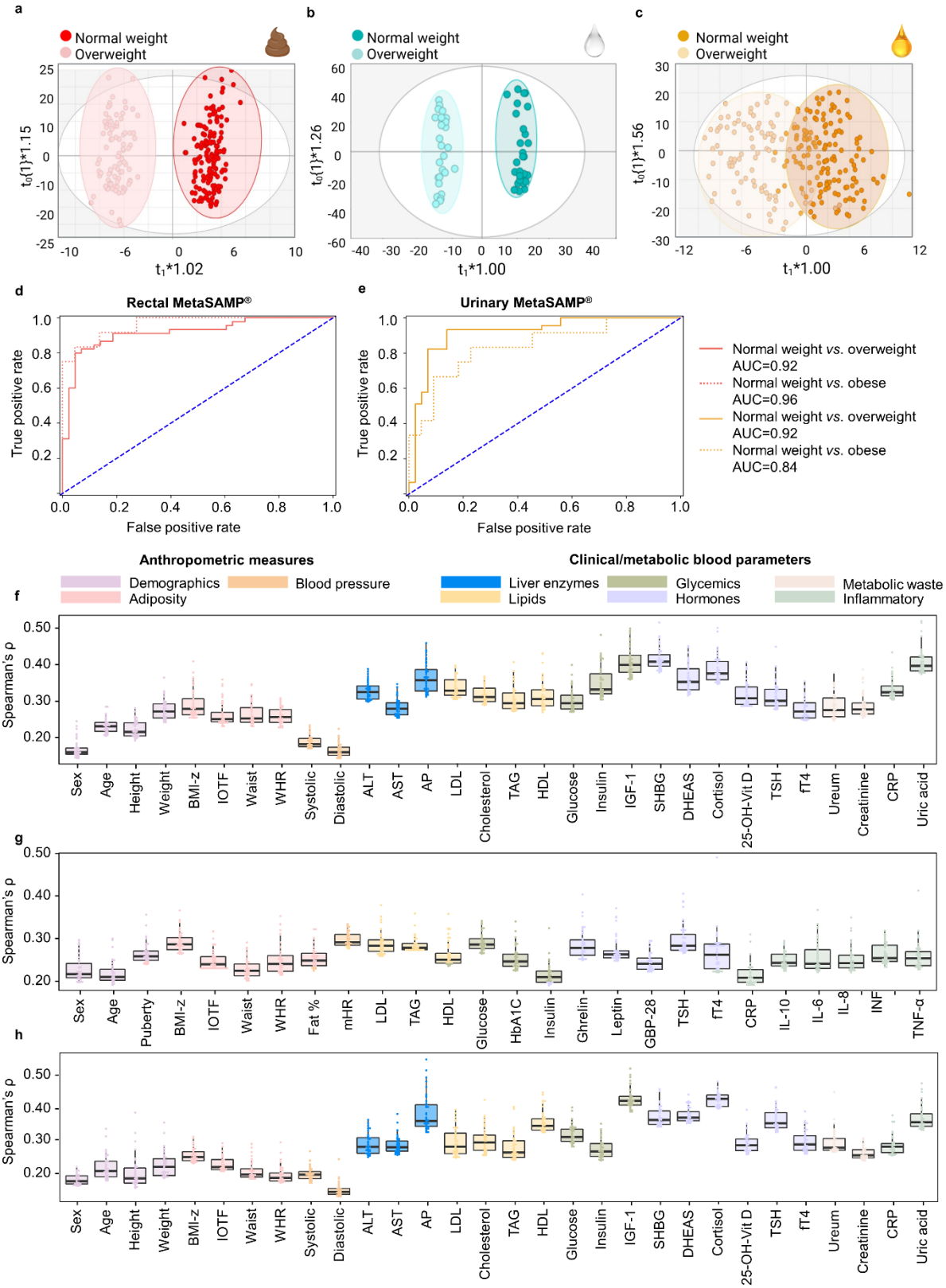

Figure 4. Biofluid-specific MetaSAMP®-LA-REIMS molecular features reflect anthropometric measures and clinical and metabolic blood markers.

(A-C) OPLS-DA score plots as obtained upon LA-REIMS fingerprinting of biofluid-specific MetaSAMPs® with clustering according to weight classification in the patient cohorts, i.e., **(A)** stool ($R^2(Y)=0.96$, $Q^2(Y)=0.63$, CV-ANOVA $p=1.15e^{-13}$), **(B)** saliva ($R^2(Y)=0.98$, $Q^2(Y)=0.53$, $p=4.05e^{-5}$) and **(C)** urine ($R^2(Y)=0.64$, $Q^2(Y)=0.58$, $p=1.68e^{-11}$). ROC curves are plotted using logistic regression analysis to visualize the predictive performance of LA-REIMS analysis in negative polarity mode with **(D)** rectal MetaSAMP® and **e.** urinary MetaSAMP® based on IOTF classification ($n=127$ with IOTF=0, $n=54$ with IOTF=1 and $n=34$ IOTF ≥ 1). Beeswarm boxplots showing the strongest observed links (anthropometrical measurements and clinical/metabolic blood metadata, *horizontal*) according to Spearman's correlation (*vertical*), with molecular features measured using the **(F)** rectal, **(G)** salivary and **(H)** urinary MetaSAMPs®. Only the 50 strongest significant correlations of molecules and parameter under observation were included, based on Spearman's ρ-value. The interior middle line in the beeswarm boxplots represents the median, lower and upper bounds of the box represent the 25th and 75th percentile values, respectively. Whiskers are drawn from the corresponding box boundary to the most extreme data point located within the box bound ± 1.5 × interquartile range. Beeswarm dots represent Spearman's correlations of individual molecular features with the parameter under investigation.

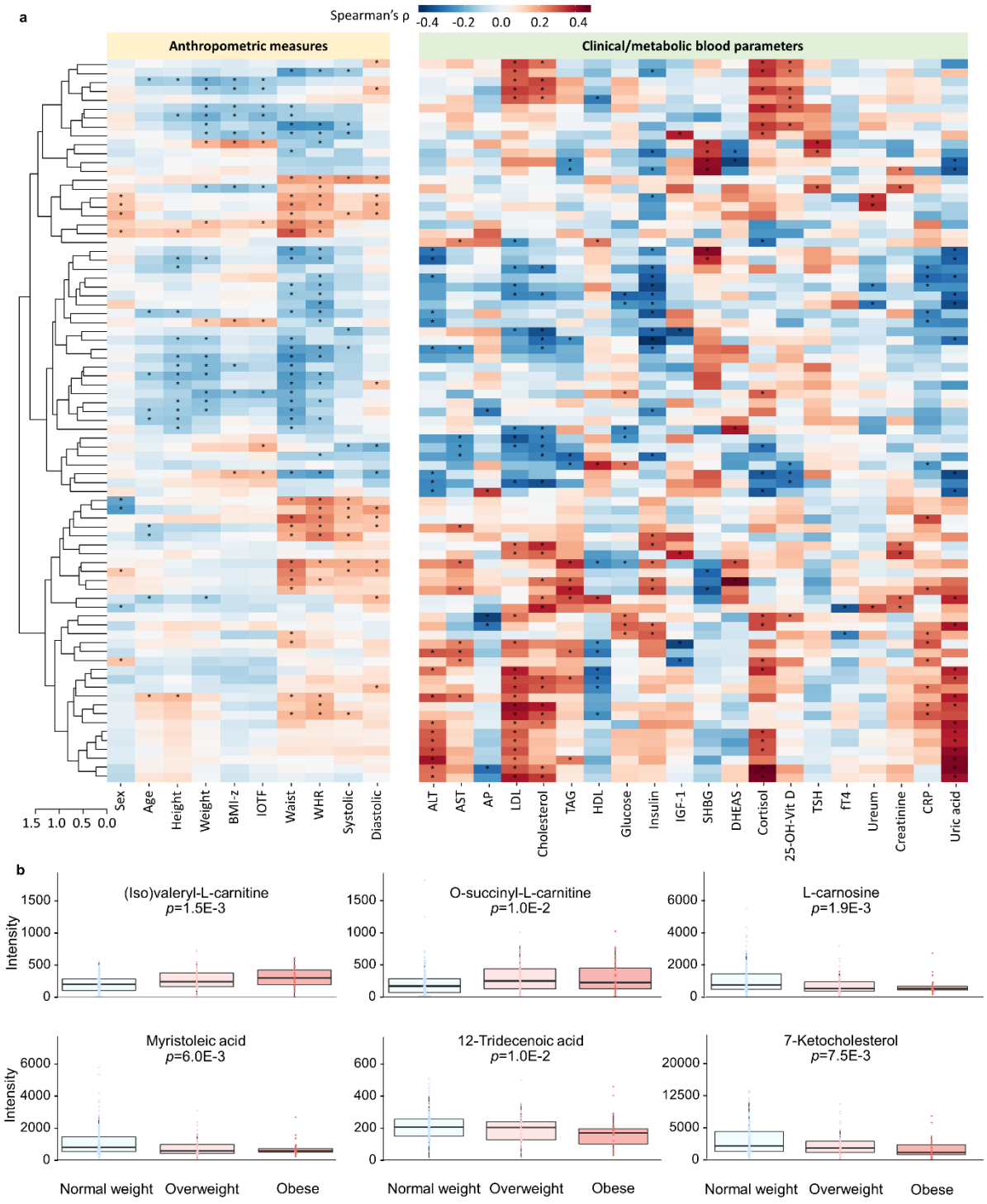

Figure 5. Metabolites detected using rectal MetaSAMP®-LA-REIMS enable individual stratification based on anthropometric and clinical blood markers.

(A) Heatmaps showing relative levels of LA-REIMS (negative ion mode)-derived molecular features that showed significant (FDR-adjusted p<0.05, marked with an asterisk) Spearman correlations with anthropometric measures and/or clinical/metabolic blood parameters from the MetaBEAse cohort. The molecular features (*n*=81 unique correlation structures) with the highest absolute correlation values and at least 4 significant associations (in-between

comparisons adjusted p values ≤0.01, using FDR correction). **(B)** Beeswarm boxplots of discriminatory features between normal weight (IOTF<1), overweight (IOTF=1) and obese (IOTF>1) children with corresponding corrected p values. The interior horizontal line represents the median value, lower and upper bounds of the box represent the 25th and 75th percentile values, respectively, and whiskers are drawn from the corresponding box boundary to the most extreme data point located within the box bound ± 1.5 × interquartile range. The beeswarm dots represent the Spearman's correlation of the individual metabolic feature intensity with the parameter under investigation. Statistical analysis was performed using a Wilcoxon rank sum test with continuity correction for the heatmap and pairwise univariate comparisons and Kruskal–Wallis with Dunn's post-hoc test for multiple comparisons.

Table 1. Demographic and anthropometric cohort findings. Data from the MetaBEAse and OPERA(*41*) cohorts comprising overweight and normal weight children.

	MetaBEAse		OPERA	
MetaSAMP®	# REIMS analyses			
Rectal	534		NA	
Salivary	NA		372	
Urinary	532		NA	
Demographics	Mean ± SD (or expressed in %)			
	# of subjects		# of subjects	
Mean age (years) ±SD	234	9 ± 2	101	14.0 ± 2
Sex	234	45% female	101	55% female
Puberty				
Tanner stage ≤1	234	100%	7	7%
Tanner stage >1			91	93%
Anthropometrics				
BMI-z scores	234		101	
Range		-3-3		-2-4
≤ -2.0 (underweight)		5 (2.1%)		1 (1.0%)
Between -2.0 and ≤ 1.0 (normal weight)		136 (58.1%)		69 (68.3%)
Between 1.0 and < 2.0 (overweight)		36 (15.4%)		19 (18.8%)
≥ 2.0 (obese)		57 (24.4%)		12 (11.9%)
IOTF	234		101	
Range		-3-3		-1-2
≤-1 (underweight)		19 (8.1%)		4 (4.0%)
0 (normal weight)		127 (54.3%)		66 (65.3%)
1 (overweight)		55 (23.5%)		20 (19.8%)
≥2 (obese)		33 (14.1%)		11 (10.9%)
WC (cm)	215	67.0 ± 12.6	101	74.6 ±10.3
WHR	214	0.49 ± 0.07	101	0.45 ± 0.07
Fat (%)	NA		98	23.8 ± 8.7
Systolic BP	215	105 ± 14.3	NA	
Diastolic BP	215	67 ± 9.6	NA	
Heart rate (bpm)	27	79.4 ± 12.2	86	77.3 ± 10.5
Clinical laboratory tests				

LDL cholesterol (mg dL^{-1})	55	97.0 ± 18.9	75	87.6 ± 21.0
Triglycerides (mg dL^{-1})	64	77.7 ± 35.5	75	81.9 ± 41.8
HDL cholesterol (mg dL^{-1})	63	50.3 ± 10.1	75	59.7 ± 13.7
Fasting plasma glucose (mg dL^{-1})	84	87.6 ± 6.7	75	88.1 ± 6.7
Cholesterol (mg dL^{-1})	64	154.9 ± 16.8	75	159.2 ± 28.1
HbA1c (%)	18	5.3 ± 0.2	76	5.3 ± 0.3
Fasting plasma insulin (pmol L^{-1})	58	80.7 ± 35.7	75	13.3 ± 9.7
TSH (mU L^{-1})	51	2.3 ± 0.8	75	2.4 ±1.1
fT4 (pmol L^{-1})	43	14.9 ± 2.4	75	15.4 ± 2.2
(hs-)CRP (mg L^{-1})	55	2.1 ± 1.6	76	1.1 ± 1.5
IL-10 (pg mL^{-1})	NA		78	0.4 ± 0.7
IL-6 (pg mL^{-1})	NA		78	0.5 ± 0.5
IL-8 (pg mL^{-1})	NA		78	10.6 ± 5.2
IFN (pg mL^{-1})	NA		78	13.8 ± 43.4
TNF (pg mL^{-1})	NA		78	1.8 ± 0.6
Polymorphonuclear cells (%)	52	49.0 ± 9.2		
Lymphocytes (%)	62	36.3 ± 9.0		
ALT (U L^{-1})	69	19.2 ± 5.6		
AST (U L^{-1})	72	26.4 ± 5.2		
AF (U L^{-1})	29	272.0 ± 60.6		
Ureum (mg dL^{-1})	65	28.1 ± 6.2		
Creatinine (mg dL^{-1})	56	0.47 ± 0.1		
Cortisol (ng mL^{-1})	47	79.0 ± 67.0		
25-hydroxyvitamin D (ng mL^{-1})	47	33.5 ± 19.9		
Uric acid (mg dL^{-1})	36	4.6 ± 0.9		
IGF-1 (µg L^{-1})	31	188.5 ± 55.8		
SHBG (nmol L^{-1})	42	49.1 ± 20.1		
DHEAS (µg dL^{-1})	33	93.9 ± 61.0		

Abbreviations: LDL, low-density lipoprotein; HDL, high-density lipoprotein; HbA1c, hemoglobin A1c; TSH, thyroid-stimulating hormone; fT4, free thyroxine; (hs)-CRP, (highly sensitive) C-reactive protein; IL, interleukin; INF, interferon; TNF, tumor necrosis factor; ALT, alanine transaminase; AST, aspartate transaminase; AF, alkaline phosphatase; IGF-1, insulin-like growth factor 1; SHBG, sex hormone-binding globulin; DHEAS, dehydroepiandrosterone sulfate.